

Experimental observation of Fermi-level flat band in novel kagome metal $CeNi_5$

Xue-Zhi Chen(陈学智), Le Wang(王乐), Shuai Zhang(张帅), Ren-Jie Zhang(张任杰), Yi-Wei Cheng(程以伟), Yu-Dong Hu(胡裕栋), Cheng-Nuo Meng(孟承诺), Zheng-Tai Liu(刘正太), Bai-Qing Lv(吕佰晴), and Yao-Bo Huang(黄耀波)

Citation: Chin. Phys. B, 2024, 33 (**8**): 087402. DOI: 10.1088/1674-1056/ad4019

What follows is a list of articles you may be interested in

Electronic structure and effective mass of pristine and Cl-doped $CsPbBr_3$

Zhiyuan Wei(魏志远), Yu-Hao Wei(魏愉昊), Shendong Xu(徐申东), Shuting Peng(彭舒婷), Makoto Hashimoto, Donghui Lu(路东辉), Xu Pan(潘旭), Min-Quan Kuang(匡泯泉), Zhengguo Xiao(肖正国), and Junfeng He(何俊峰)
Chin. Phys. B, 2024, 33 (**5**): 057403. DOI: 10.1088/1674-1056/ad3c31

Conservation of the particle-hole symmetry in the pseudogap state in optimally-doped $Bi_2Sr_2CuO_{6+\delta}$ superconductor

Hongtao Yan(闫宏涛), Qiang Gao(高强), Chunyao Song(宋春尧), Chaohui Yin(殷超辉), Yiwen Chen(陈逸雯), Fengfeng Zhang(张丰丰), Feng Yang(杨峰), Shenjin Zhang(张申金), Qinjun Peng(彭钦军), Guodong Liu(刘国东), Lin Zhao(赵林), Zuyan Xu(许祖彦), and X. J. Zhou(周兴江)
Chin. Phys. B, 2022, 31 (**8**): 087401. DOI: 10.1088/1674-1056/ac7214

Measurement of electronic structure in van der Waals ferromagnet $Fe_{5-x}GeTe_2$

Kui Huang(黄逵), Zhenxian Li(李政贤), Deping Guo(郭的坪), Haifeng Yang(杨海峰), Yiwei Li(李一苇),Aiji Liang(梁爱基), Fan Wu(吴凡), Lixuan Xu(徐丽璇), Lexian Yang(杨乐仙), Wei Ji(季威),Yanfeng Guo(郭艳峰), Yulin Chen(陈宇林), and Zhongkai Liu(柳仲楷)
Chin. Phys. B, 2022, 31 (**5**): 057404. DOI: 10.1088/1674-1056/ac5c3c

Surface-induced orbital-selective band reconstruction in kagome superconductor CsV_3Sb_5

Linwei Huai(淮琳崴), Yang Luo(罗洋), Samuel M. L. Teicher, Brenden R. Ortiz, Kaize Wang(王铠泽),Shuting Peng(彭舒婷), Zhiyuan Wei(魏志远), Jianchang Shen(沈建昌), Bingqian Wang(王冰倩), Yu Miao(缪宇),Xiupeng Sun(孙秀鹏), Zhipeng Ou(欧志鹏), Stephen D. Wilson, and Junfeng He(何俊峰)
Chin. Phys. B, 2022, 31 (**5**): 057403. DOI: 10.1088/1674-1056/ac4f50

Dispersion of neutron spin resonance mode in $Ba_{0.67}K_{0.33}Fe_2As_2$

Tao Xie(谢涛), Chang Liu(刘畅), Tom Fennell, Uwe Stuhr, Shi-Liang Li(李世亮), and Hui-Qian Luo(罗会仟)
Chin. Phys. B, 2021, 30 (**12**): 127402. DOI: 10.1088/1674-1056/ac3651

Experimental observation of Fermi-level flat band in novel kagome metal $CeNi_5$

Xue-Zhi Chen(陈学智)[1,2,3], Le Wang(王乐)[4,5], Shuai Zhang(张帅)[6], Ren-Jie Zhang(张任杰)[2,3,7], Yi-Wei Cheng(程以伟)[1,2,3], Yu-Dong Hu(胡裕栋)[2], Cheng-Nuo Meng(孟承诺)[1,3], Zheng-Tai Liu(刘正太)[10], Bai-Qing Lv(吕佰晴)[2,8,9,†], and Yao-Bo Huang(黄耀波)[10,1,3,‡]

[1] *Shanghai Institute of Applied Physics, Chinese Academy of Sciences, Shanghai* 201800, *China*
[2] *Tsung-Dao Lee Institute, Shanghai Jiao Tong University, Shanghai* 200240, *China*
[3] *University of Chinese Academy of Sciences, Beijing* 100049, *China*
[4] *Shenzhen Institute for Quantum Science and Engineering, Southern University of Science and Technology, Shenzhen* 518055, *China*
[5] *International Quantum Academy, Shenzhen* 518048, *China*
[6] *Institute of Theoretical Physics, Chinese Academy of Sciences, Beijing* 100190, *China*
[7] *Beijing National Laboratory for Condensed Matter Physics and Institute of Physics, Chinese Academy of Sciences, Beijing* 100190, *China*
[8] *School of Physics and Astronomy, Shanghai Jiao Tong University, Shanghai* 200240, *China*
[9] *Zhangjiang Institute for Advanced Study, Shanghai Jiao Tong University, Shanghai* 200240, *China*
[10] *Shanghai Synchrotron Radiation Facility, Shanghai Advanced Research Institute, Chinese Academy of Sciences, Shanghai* 201204, *China*

(Received 10 February 2024; revised manuscript received 16 March 2024; accepted manuscript online 18 April 2024)

Kagome materials are a class of material with a lattice structure composed of corner-sharing triangles that produce various exotic electronic phenomena, such as Dirac fermions, van Hove singularities, and flat bands. However, most of the known kagome materials have a flat band detached from the Fermi energy, which limits the investigation of the emergent flat band physics. In this work, by combining soft x-ray angle-resolved photoemission spectroscopy (ARPES) and the first-principles calculations, the electronic structure is investigated of a novel kagome metal $CeNi_5$ with a clear dispersion along the k_z direction and a Fermi level flat band in the Γ–K–M–Γ plane. Besides, resonant ARPES experimental results indicate that the valence state of Ce ions is close to 4^+, which is consistent with the transport measurement result. Our results demonstrate the unique electronic properties of $CeNi_5$ as a new kagome metal and provide an ideal platform for exploring the flat band physics and the interactions between different types of flat bands by tuning the valence state of Ce ions.

Keywords: ARPES, kagome lattice, band structure, flat band

PACS: 74.25.Jb, 71.27.+a, 73.20.–r, 79.60.–i **DOI:** 10.1088/1674-1056/ad4019

1. Introduction

Kagome materials are a class of material that has a special lattice structure composed of corner-sharing triangles, forming a planar tiling pattern. Due to its unique crystal structure, the kagome lattice naturally exhibits Dirac fermions, van Hove singularities (vHs), and flat bands in its electronic structure (Fig. 1(c)) which has attracted widespread attention due to its rich and exotic physical phenomena.[1,2]

Firstly, the Dirac fermions which are described by the Dirac equation, can host the topological non-trivial properties of the band structure.[3] In the kagome lattice, the Dirac fermions can form different topological phases, such as Chern insulators, anomalous Hall effects, and Weyl semimetals by symmetry breaking, spin–orbit coupling, or other interactions.[4–7] Secondly, vHss located in the vicinity of the Fermi energy (E_F) can provide a high density of states in electronic structure, which can induce Fermi surface instability and play a key role in forming long-range ordered phases, such as charge/spin density waves and superconductivity.[8–10] The flat band with non-dispersive electronic structures, which is induced by destructive quantum interference, is another key feature of the kagome lattice.[11] This feature provides an extremely high density of states in a very small energy range which enhances the electron–electron interactions, making it a popular platform for investigating the novel properties in strongly correlated many-body systems, such as high-temperature superconductivity,[12] fractional quantum Hall effect,[13] and Wigner crystal.[14]

A variety of kagome lattice materials have been investigated extensively, such as Fe_3Sn_2, $Co_3Sn_2S_2$, CoSn, $LnMn_6Sn_6$ (Ln = Y, Gd), ATi_3Bi_5 (A = Rb, Cs), and AV_3Sb_5 (A = K, Rb, Cs), exhibiting intriguing electronic properties, such as massive Dirac fermion, magnetic Weyl fermions, Chern magnets, charge density wave, nematic phases, and superconductivity.[4–6,15–21] However, the flat band structure in these materials is either not observed or only observed far from the E_F (typically about hundreds of meV), which hinders the exploration of flat band physics.

†Corresponding author. E-mail: baiqing@sjtu.edu.cn
‡Corresponding author. E-mail: huangyaobo@sari.ac.cn

© 2024 Chinese Physical Society and IOP Publishing Ltd

In this work, we comprehensively study the electronic structure of a novel kagome metal $CeNi_5$ by combining first-principles calculations and angle-resolved photoemission spectroscopy (ARPES). We directly map out the band dispersion and the Fermi surface of this material, revealing the a flat band at E_F, which can significantly affect the charge transport properties. Our results demonstrate the unique electronic properties of $CeNi_5$ as a novel kagome metal and provide a new platform for exploring flat band physics in correlated systems.

2. Methods

2.1. Angle-resolved photoemission spectroscopy

High-resolution soft x-ray ARPES measurements were performed at the "Dreamline" beamline of the Shanghai Synchrotron Radiation Facility (SSRF) with a Scienta Omicron DA30L analyzer. The photon energy ranged from 330 eV to 520 eV, and the combined (beamline and analyzer) experimental energy resolution was in a ranges of 40 meV–80 meV. The angular resolution of the DA30L analyzer was 0.1°. The beam spot at the experimental condition had a cross-sectional size of 80 μm by 80 μm. Fresh surfaces were obtained by cleaving $CeNi_5$ single crystals *in situ* under an ultrahigh vacuum base pressure below 5.0×10^{-11} Torr (1 Torr = 1.33322×10^2 Pa).

2.2. Sample synthesis

According to the Ce–Ni binary phase diagram, $CeNi_5$ undergoes homogeneous melting around 1360 °C. Therefore, we synthesized this crystal phase by employing the arc melting technique in a WK-II Non-Consumable Vacuum Arc Furnace (Physcience Opto-electronics Co., Ltd., Beijing). High-purity cerium blocks with the surface oxide layer polished and nickel rods were used as raw materials, prepared in a molar ratio of Ce:Ni=1:5, totaling approximately 12 g, and placed into the melting device. After standard purging operations, argon gas was introduced. Initially, titanium metal blocks were premelted for 5 min to remove residual oxygen from the chamber as much as possible, followed by the melting of our raw materials. The current was first increased to 160 A and maintained for 2 min to ensure complete melting and mixing. Then, the current was reduced to 130 A and maintained for 2 min., followed by a further reduction to 110 A and maintained for 5 min. Finally, the current was manually controlled to decrease in steps of about 1 A/min until reaching 50 A, and the current was maintained at 10 A for 10 min till ending the melting process. A large ingot was obtained, lightly crushed with a mortar and pestle, yielding well-crystallized, metallic lustrous single-crystal grains ranging from 1 mm to 2 mm in size. As shown in Fig. 1(d), single crystal grains were selected, ground into powder, and characterized by using powder x-ray diffraction (XRD), confirming that the crystal structure belongs to the space group of $P6/mmm$ (No. 191) for $CeNi_5$.

2.3. Calculation

We calculated the electronic structure and the atomic orbital weighted band structure by using the Vienna *ab initio* simulation package (VASP).[22,23] The projector-augmented-wave (PAW) method[24,25] and the Perdew–Burke–Ernzerhof (PBE) exchange–correlation functional[26] were used in the calculation. We set the plane-wave cutoff energy to 500 eV, and a $9\times9\times11$ Γ-centered Monkhorst–Pack was used to sample the Brillouin zone (BZ) in the self-consistent-field (SCF) calculation.

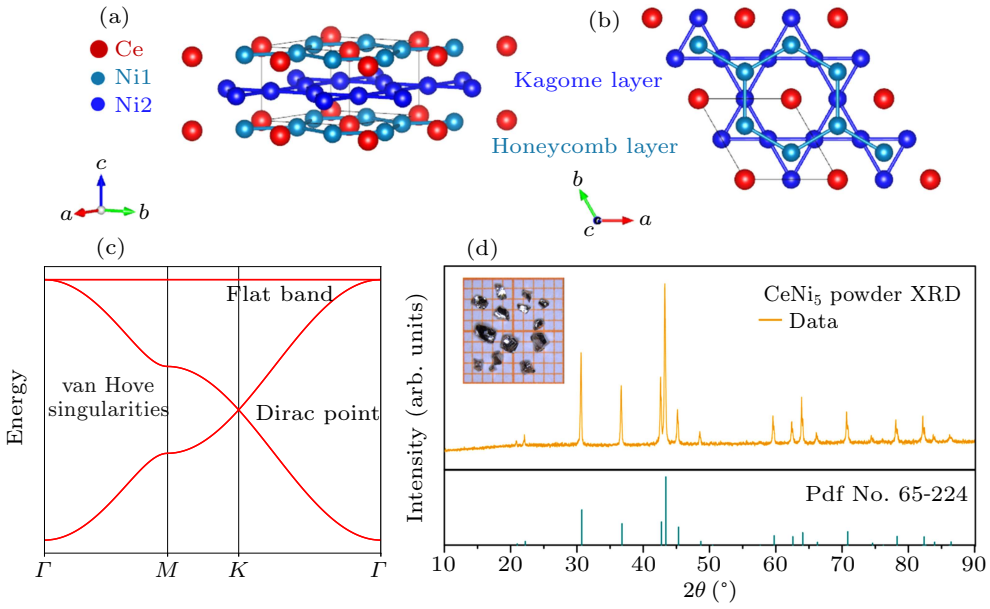


Fig. 1. (a) Crystal structure of $CeNi_5$. Ce, Ni1, and Ni2 atoms, represented by red, cerulean blue, and blue balls, respectively. (b) Top view of crystal structure of $CeNi_5$. Ni1 atoms form a honeycomb sublattice, and Ni2 atoms form a kagome sublattice, respectively. (c) Tight-binding band structure of kagome lattice, exhibiting Dirac point at the K point, Van Hove singularities at the M point, and a flat band. (d) Powder XRD pattern of $CeNi_5$, with inset showing morphology of $CeNi_5$ single crystal. Panels (a) and (b) were generated by Vesta.[27]

3. Results

$CeNi_5$ crystallizes into $CaCu_5$ hexagonal crystal structure with space group $P6/mmm$ (No. 191).[28] The Ce atom occupies the high symmetry 1*a* (0, 0, 0) Wyckoff position, while the Ni atoms are located at the 2*c* (1/3, 2/3, 0) and 3*g* (1/2, 0, 1/2) positions. In $CeNi_5$, Ni forms two sublattices: Ni atoms at 2*c* form a honeycomb sublattice, and Ni atoms at 3*g* form a kagome sublattice as shown in Figs. 1(a) and 1(b).

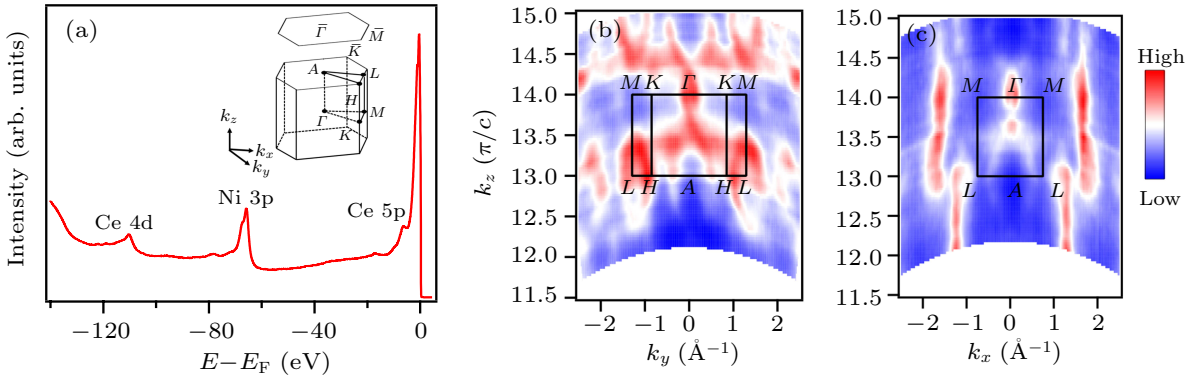


Fig. 2. (a) Core-level photoemission spectrum showing characteristic peaks of Ce and Ni elements, with inset showing hexagonal BZ and corresponding surface BZ of $CeNi_5$. (b), (c) Constant energy map of ARPES data collected in vertical (b) *Γ*–*K*–*M*–*A*–*H*–*L* plane and (c) *Γ*–*M*–*A*–*L* plane with $E_B = 0.15$ eV in photon energy range from 350 eV to 520 eV, with inner potential $V_0 = 17$ eV and lattice constant $c = 4.01$ Å. All the data were collected at 20 K with s polarization.

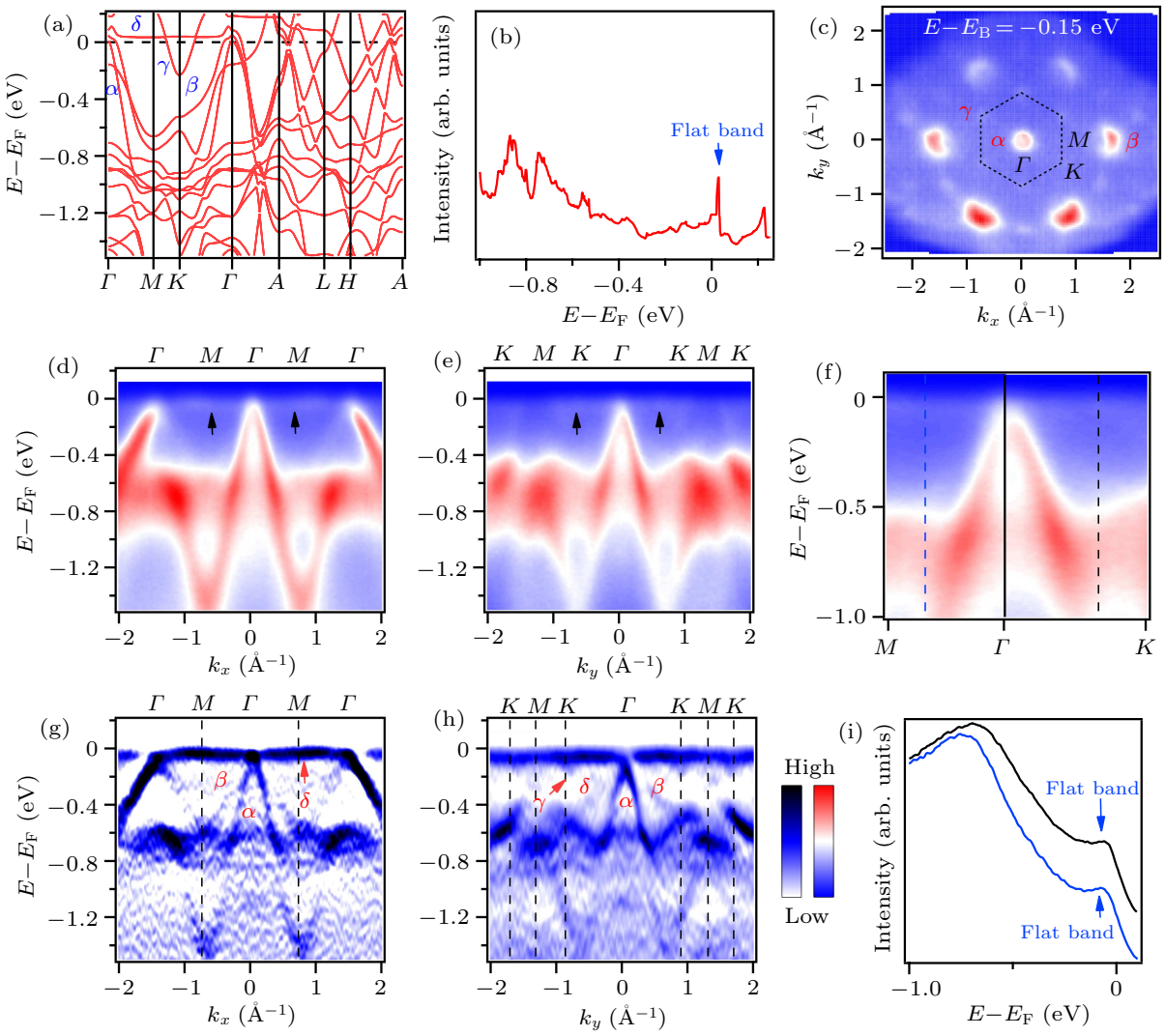


Fig. 3. (a) Calculated bulk bands of $CeNi_5$ along high-symmetry lines with spin–orbit coupling: One flat band (δ), two hole-like bands (α, β), and one electron-like band (γ). (b) Calculated density of states, with a peak raised by flat band emergy near E_F. (c) Intensity plot of ARPES data in *Γ*–*K*–*M* plane at $E_B = -0.15$ eV and $h\nu = 445$ eV. Photoemission intensity distributions along (d) *Γ*–*M* direction, and (e) *Γ*–*K* direction. (f) Band structure along *M*–*Γ*–*K* direction. 2D curvature intensity plot along (g) *Γ*–*M* direction, and *Γ*–*K* direction. (i) EDCs at the momentum location labeled by blue dash lines and black line in panel (f). All the data were collected at 20 K with s polarization.

Firstly, we perform x-ray photoemission spectrum experiments as shown in Fig. 2(a) where Ce and Ni core-level peaks are observed, confirming the chemical composition of our sample. Next, we investigate the electronic structure of $CeNi_5$ by performing systematic soft x-ray ARPES measurements on the (001) surface. it is worth noting that the data obtained by using vacuum ultraviolet light (VUV) are blurry, even though the fresh surfaces are obtained by cleaving *in situ*. In contrast, the data obtained by using soft x-rays clearly show the band dispersion and Fermi surfaces. A possible explanation for this is that the cleaved mirror-like surface has a very small flat area, which impedes the detection of the bulk electronic structure by VUV due to limited penetration depth in this photon energy range while soft x-rays enhance the bulk sensitivity of the ARPES measurements significantly.[29] Besides, owing to the Heisenberg uncertainty principle,[29] higher energy photons enhance the intrinsic ARPES momentum resolution perpendicular to the surface, thus enhancing the extraction of the electronic structures of three-dimensional (3D) systems like in the case of MoP and WC.[30,31]

As $CeNi_5$ is a typical 3D material, it is essential to elucidate the bulk-band structure in the 3D BZ. For this purpose, we carry out $h\nu$-dependent ARPES measurements on the (001) surface at the normal emission setup to observe the band dispersion along k_z direction (parallel to the c axis). Figures 2(b) and 2(c) display the constant energy plots recorded on the (001) surfaces along Γ–K and Γ–M, respectively, and show obvious k_z dispersion, thus confirming its bulk property. The inner potential value V_0 is estimated to be 17 eV from the periodicity of the band dispersion along k_z.

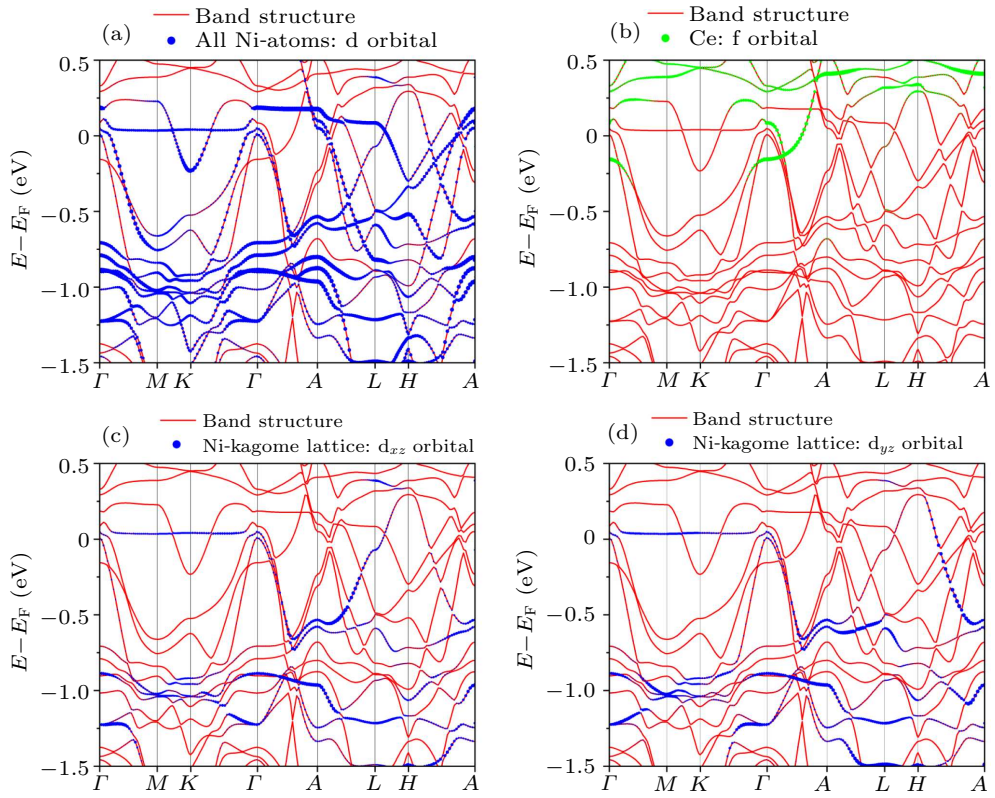


Fig. 4. Calculated orbital-projection band-structures of $CeNi_5$ with spin–orbit coupling, with orbital weights represented by both color and band size. (a) Calculated d orbital weights of all Ni atoms. (b) Calculated f orbital weights of Ce atoms. (c)–(d) The calculated (c) d_{xz} orbital weight and (d) d_{yz} orbital weight of Ni atoms formed kagome lattice.

The calculated band structure of $CeNi_5$ is plotted in Fig. 3(a). The electronic structure of $CeNi_5$ around E_F shows three main features: an electron-like band, named γ, centered at the K point, hole-like bands centered at the Γ point denoted by α and β, and in particular, a flat band represented by δ positioned slightly above E_F along the high-symmetry direction of Γ–M–K–Γ, which induces a peak in the calculated density of states, denoted by the blue arrow (see Fig. 3(b)). To probe this flat band, we perform ARPES measurements at a value of photon energy of $h\nu = 445$ eV, which corresponds to the $k_z \sim 0$ plane. Figure 3(c) displays the constant energy intensity maps of the ARPES data at $E_B = -0.15$ eV which is composed of two hole-like pockets (α and β) centered at the Γ point, and an electron-like pocket (γ) at the K point (Fig. 3(c)). The spectral intensity of the β band in the first BZ is much lower than that in higher BZs, whereas the spectral intensity of the α band in the first BZ is much stronger than that in higher BZs, normally due to the matrix element effect of photoemission. To eliminate the strong intensity variation and focus on the band dispersion, we plot the experimental results along the Γ–M direc-

tion and the Γ–K direction in the first BZ (see Fig. 3(f)). The flat band δ is observed near E_F along both the Γ–M direction and the Γ–K direction (see Figs. 3(d) and 3(e)) as indicated by black arrows. The flat band δ is more clearly visible in the corresponding secondary derivative plots of the ARPES data (see Figs. 3(g) and 3(h)).[32] The extracted energy distribution curves (EDCs) whose momentum location is represented by the blue line, and black-dash line in Fig. 3(f) show an obvious hump feature caused by the flat band near the E_F displayed in Fig. 3(i). The electronic structure of $CeNi_5$ is shown in Fig. 3, showing dispersive bands crossing the E_F, which is in accordance with the reported metallic behaviors.[33]

To analyze the origin of the observed flat band, we analyze the systematic orbital-projected band structure , and the results are shown in Fig. 4. It can be found that the flat band mainly arises from the d_{xz} orbital and d_{yz} orbital on the kagome lattice formed by Ni atoms (Figs. 4(c) and 4(d)) and most of the f orbital bands are above E_F (Fig. 4(b)) (see supplementary materials for more DFT results). It is worth mentioning that the calculated flat band in Fig. 3(a) shows obvious k_z dispersion, which makes it possible to identify this band in other k_z planes (see supplementary materials for further details). Our ARPES experimental results are highly consistent with our theoretical calculations, which directly confirms the existence of a flat band near the E_F in this kagome metal $CeNi_5$.

4. Discussion

Besides the kagome lattice, the flat band electronic structure can also be realized by other mechanisms, such as manipulation of electrons in some artificial structures, and strong localization of electrons. A well-known example is magic-angle twisted bilayer graphene, where the electrons are trapped in the moiré pattern resulting from the rotation angle of two layers of graphene, leading to a flat band near the E_F and inducing both the correlated insulator states[34] and the strong-coupling superconductivity.[35] Another example is heavy fermion material with strongly localized electrons.[36] Hence, it is a natural and intriguing idea to explore the interaction between different flat bands, such as the kagome flat band and the heavy-fermion flat band.

Ce-based compounds are typical heavy fermion materials with f electron flat bands located at the E_F.[37–39] In $CeNi_5$, it is anticipated that the f electron flat band exists at E_F. To probe the possible interaction between the kagome flat band and the f electron flat band, we perform comparative ARPES measurements under the off-resonant conditions (110 eV, 115 eV) and on-resonant condition (121 eV) condition (Figs. 5(a)–5(c)). However, $CeNi_5$ deviates from the typical Ce-based heavy fermion system behaviors, as neither the on-resonant spectrum nor the off-resonant spectrum shows evident flat features, and the on-resonant spectrum exhibits few discernible enhancements of spectral intensity (Fig. 5(d)). Indeed, the electronic Sommerfeld coefficient γ of $CeNi_5$ is only 40 mJ/(mol·K^2),[40] significantly lower than that of the typical heavy fermion compound $CeAl_3$,[41] which has a value of 1.62 J/(mol·K^2). From experiments of the lattice parameters and x-ray absorption, the valence state of Ce in $CeNi_5$ is close to 4^+[42] without localized f electrons, while the valence state of Ce of the typical Ce-based heavy fermion system is 3^+ with one f electron. Furthermore, the energy scales of Ce 3^+ and Ce 4^+ are very similar, which facilitates the tuning of the valence state of Ce ions in $CeNi_5$ from 3^+ to 4^+ by changing external parameters,[40] such as pressure, magnetic field, and doping in the future study. This may induce interaction between the kagome flat band and the f electron, giving rise to novel physical phenomena in $CeNi_5$.

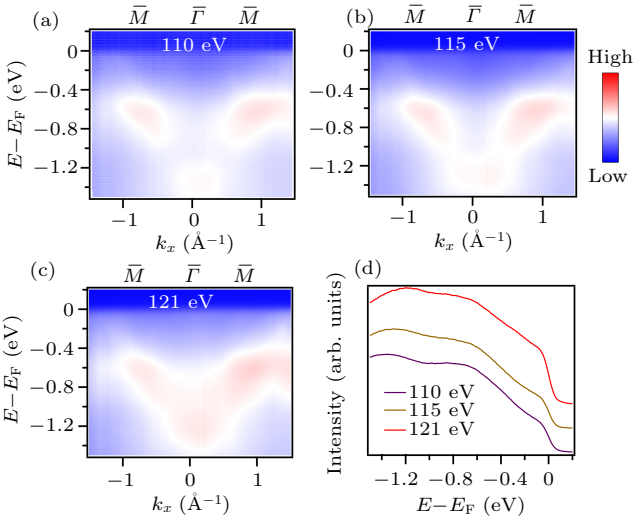


Fig. 5. (a)–(c) Photoemission intensity distributions along $\bar{\Gamma}$–$\bar{M}$ with off-resonant photon energy of (a) 110 eV, (b) 115 eV, and on-resonant photon energy of (c) 121 eV. (d) EDCs at the $\bar{\Gamma}$ center for photon energy of 110 eV, 115 eV, and 121 eV.

5. Conclusions

We have comprehensively investigated the band structures of a novel kagome metal $CeNi_5$ by combining first-principles calculations and soft x-ray ARPES experiments. we reveal the electronic structure of $CeNi_5$ with obvious k_z dispersion. More importantly, our results indicate that a flat band mainly arises from the d_{yz} and d_{xz} orbitals on the kagome lattice formed by Ni atoms located near the E_F in Γ–K–M–Γ plane in momentum space, which is rare compared with other kagome lattice materials. Resonant ARPES experiments indicate the valence of Ce ion is close to 4+ which is consistent with transport experimental result. Our results provide a new kagome metal as a platform for exploring the kagome flat band

physics and interaction between different types of flat bands by tuning the valence state of Ce ions in $CeNi_5$.

Acknowledgements

We thank Shunye Gao and Gexing Qu for their assistance in the ARPES experiments, and also Hongming Weng and Zhida Song for fruitful discussion.

Project support by the Science Fund from Shanghai Committee of Science and Technology, China (Grant No. 23JC1403300), the Shanghai Municipal Science and Technology Major Project, China, the TDLI Starting up Grant, the National Natural Science Foundation of China (Grant Nos. 12374063, 12204223, and 23Z990202580), the Fund from the Ministry of Science and Technology of China (Grant No. 2023YFA1407400), the Shanghai Natural Science Fund for Original Exploration Program, China (Grant No. 23ZR1479900), and Shanghai Talent Program, China.

References

[1] Yin J X, Lian B and Hasan M Z 2022 *Nature* **612** 647
[2] Wang Y, Wu H, McCandless G T, Chan, J Y and Ali M 2023 *Nat. Rev. Phys.* **5** 635
[3] Wang Z J, Sun Y, Chen X Q, Franchini C, Xu G, Weng H M, Dai X and Fang Z 2012 *Phys. Rev. B* **85** 195320
[4] Ye L D, Kang M G, Liu J W, Cube F V, Wicker C R, Suzuki T, Jozwiak C, Bostwick A, Rotenberg E, Bell D C, Fu L, Comin R and Checkelsky J G 2018 *Nature* **555** 638
[5] Yin J X, Ma W L, Cochran T A, *et al*. 2020 *Nature* **583** 533
[6] Liu D F, Liang A J, Liu E K, Xu Q N, Li Y W, Chen C, Pei D, Shi W J, Mo S K, Dudin P, Kim T, Cacho C, Li G, Sun Y, Yang L X, Liu Z K, Parkin S S P, Felser C and Chen Y L 2019 *Science* **365** 1282
[7] Liu E K, Sun Y, Kumar N, *et al*. 2018 *Nat. Phys.* **14** 1125
[8] Markiewicz, R S 1997 *J. Phys. Chem. Solids* **58** 1179
[9] Wang W S, Li Z Z, Xiang Y Y and Wang Q H 2013 *Phys. Rev. B* **87** 115135
[10] Kiesel M L, Platt C and Thomale R 2013 *Phys. Rev. Lett.* **110** 126405
[11] Regnault N, Xu Y F, Li M R, Ma, D S, Jovanovic M, Yazdani A, Parkin S P, Felser C, Schoop L M, Ong N P, Cava R J, Elcoro L, Song Z D and Bernevig B A 2022 *Nature* **603** 824
[12] Miyahara S, Kusuta S and Furukawa N 2007 *Physica C* **460–462** 1145
[13] Tang E, Mei J W and Wen X G 2011 *Phys. Rev. Lett.* **106** 236802
[14] Wu C, Bergman D, Balents L and Das Sarma S 2007 *Phys. Rev. Lett.* **99** 070401
[15] Kang M G, Fang S A, Kim K J, Ortiz B R, Ryu S H, Kim J M, Yoo J G, Sangiovanni G, Sante D D, Park B G, Jozwiak C, Bostwick A, Rotenberg E, Kaxiras E, Wilson S D, Park J H and Comin R 2022 *Nat. Phys.* **18** 301
[16] Nie L P, Sun K L, Ma W, *et al*. 2022 *Nature* **604** 59
[17] Ortiz B R, Teicher S M L, Hu Y, Zuo J L, Sarte P M, Schueller E C, Abeykoon A M M, Krogstad M J, Rosenkranz S, Osborn R, Seshadri R, Balents L, He J F and Wilson S D 2020 *Phys. Rev. Lett.* **125** 247002
[18] Jiang Z C, Liu Z T, Ma H Y, Xia W, Liu Z H, Liu J S, Cho S, Yang Y C, Ding J Y, Liu J Y, Huang Z, Qiao Y X, Shen J J, Jing W C, Liu X Q, Liu J P, Guo Y F and Shen D W 2023 *Nat. Commun.* **14** 4892
[19] Liu Z Z, Li M, Wang Q, Wang G W, Wen C H P, Jiang K, Lu X, Yan S C, Huang Y B, Shen D W, Yin J X, Wang Z P, Lei H C and Wang S C 2020 *Nat. Commun.* **11** 4002
[20] Li M, Wang Q, Wang G W, Yuan Z H, Song W H, Lou R, Liu Z T, Huang Y B, Liu Z H, Lei H C, Yin Z P and Wang S C 2021 *Nat. Commun.* **12** 3129
[21] Liu Z H, Zhao N N, Li M, Yin Q W, Wang Q, Liu Z T, Shen D W, Huang Y B, Lei H C, Liu K and Wang S C 2021 *Phys. Rev. B* **104** 115122
[22] Kresse G and Furthmüller J 1996 *Phys. Rev. B* **54** 11169
[23] Kresse G and Furthmüller J 1996 *Comput. Mater. Sci.* **6** 15
[24] Blöchl P E 1994 *Phys.Rev. B* **50** 17953
[25] Kresse G and Joubert D 1999 *Phys. Rev. B* **59** 1758
[26] Perdew J P, Burke K and Ernzerhof M 1996 *Phys. Rev. Lett.* **77** 3865
[27] Momma K and Izumi F 2011 *J. Appl. Crystallogr.* **44** 1272
[28] Wang J, Jorda J L, Pisch A and Flükiger R 2006 *Intermetallics* **14** 695
[29] Lv B Q, Qian T and Ding H 2019 *Nat. Rev. Phys.* **1** 609
[30] Ma J Z, He J B, Xu Y F, *et al*. 2018 *Nat. Phys.* **14** 349
[31] Lv B Q, Feng Z L, Xu Q N, Gao X, Ma J Z, Kong L Y, Richard P, Huang Y B, Strocov V N, Fang C, Weng H M, Shi Y G, Qian T and Ding H 2017 *Nature* **546** 627
[32] Zhang P, Richard P, Qian T, Xu Y M, Dai X and Ding H 2011 *Rev. Sci. Instrum.* **82** 043712
[33] Marzouk N, Craig R S and Wallace W E 1973 *J. Phys. Chem. Solids* **34** 15
[34] Cao Y, Fatemi V, Demir Ahmet, Fang S A, Tomarken S L, Luo J Y, Sanchez-Yamagishi J D, Watanabe K J, Taniguchi T, Kaxiras E, Ashoori R C and Jarillo-Herrero P 2018 *Nature* **556** 80
[35] Cao Y, Fatemi V, Fang S A, Watanabe K, Taniguchi T, Kaxiras E and Jarillo-Herrero P 2018 *Nature* **556** 43
[36] Stewart G R 1984 *Rev. Mod. Phys.* **56** 755
[37] Poelchen G, Rusinov I P, Schulz S, *et al*. 2022 *ACS Nano* **16** 3573
[38] Chen Q Y, Xu D F, Niu X H, *et al*. 2017 *Phys. Rev. B* **96** 045107
[39] Chen Q Y, Xu D F, Niu X H, Peng R, Xu H C, Wen C H P, Liu X, Shu L, Tan S Y, Lai X C, Zhang Y J, Lee H, Strocov V N, Bisti F, Dudin P, Zhu J X, Yuan H Q, Kirchner S and Feng D L 2018 *Phys. Rev. Lett.* **120** 066403
[40] Musil O, Svoboda P and Sechovský V 2005 *Physica B* **359–361** 281
[41] Andres K, Graebner J E and Ott H R 1975 *Phys. Rev. Lett.* **35** 1779
[42] Coldea M, Andreica D, Bitu M and Crisan V 1996 *J. Magn. Magn. Mater.* **157–158** 627